Anna Takácsi-Nagy[1]
Ferenc Kilár[2]
Wolfgang Thormann[3]

[1]Faculty of Pharmacy,Institute of Pharmaceutical Technology and Biopharmacy, University of Pécs, Pécs, Hungary
[2]Institute of Bioanalysis, Medical School and Szentágothai Research Center, University of Pécs, Pécs, Hungary
[3]Institute for Infectious Diseases, University of Bern, Bern, Switzerland

Received November 17, 2021
Revised December 2, 2021
Accepted December 3, 2021

Research Article

The effect of pH adjusted electrolytes on capillary isoelectric focusing assessed by high-resolution dynamic computer simulation

The effect of the composition of electrolytes on capillary IEF is assessed for systems with carrier ampholytes covering two pH units and with catholytes of decreased pH, anolytes of increased pH, and both electrode solutions with adjusted pH values. For electrolytes composed of formic acid as anolyte and ammonium hydroxide as catholyte, simulation is demonstrated to provide the expected IEF system in which analytes with p*I* values within the formed pH gradient are focused and become immobile. Addition of formic acid to the catholyte results in the formation of an isotachophoretic zone structure that migrates toward the cathode. With ammonium hydroxide added to the anolyte migration occurs toward the anode. In the two cases, all carrier components and amphoteric analytes migrate isotachophoretically as cations or anions, respectively. The data reveal that millimolar amounts of a counter ion are sufficient to convert an IEF pattern into an ITP system. With increasing amounts of the added counter ion, the overall length of the migrating zone structure shrinks, the range of the pH gradient changes, and the migration rate increases. The studied examples indicate that systems of this type reported in the literature should be classified as ITP and not IEF. When both electrolytes are titrated, a non-uniform background electrolyte composed of formic acid and ammonium hydroxide is established in which analytes migrate according to local pH and conductivity without forming IEF or ITP zone structures. Simulation data are in qualitative agreement with previously published experimental data.

Keywords:
Carrier ampholytes / Electrolytes / Isoelectric focusing / Isotachophoresis / Simulation
DOI 10.1002/elps.202100367

1 Introduction

IEF is a high-resolution analytical method in which amphoteric substances are separated based on differences in isoelectric points. Most commonly, carrier ampholytes are added to the sample and form, under the influence of an electric field, a natural pH gradient whose pH values increase in the direction of the cathode [1]. In IEF performed in open-tubular capillaries (CIEF), carrier and sample components are typically injected as a homogenous mixture throughout a column with minimized electroosmosis and CIEF is carried out in two steps: the separation or focusing step and the mobilization step during which the whole pattern is mobilized across a detector placed toward or at the capillary end [2–5]. Mobilization can be achieved by electrophoresis, applied hydrodynamic flow, or a combination of these principles. Electrophoretic (also referred to as chemical) mobilization toward the anode is accomplished by replacing the anolyte (typically an acid) with a base or adding a cation or salt in the anolyte. Conversely, cathodic mobilization can be achieved when the catholyte is replaced by an acid or via the addition of an anion to the catholyte [3,6,7]. Electrophoretic mobilization is based on each ampholyte's changed charge state caused by the gradual ion penetration from the electrode chamber through the pH gradient. The ampholytes become positively (mobilization toward cathode) or negatively (mobilization toward anode) charged. The migrating zone structure formed during this process represents ITP [8]. CIEF in the absence of EOF can also be executed as a one step process via use of an instrument that features whole column imaging, i.e., an array or scanning detector that is capable of monitoring the ongoing separation process and the focused samples [9,10].

Alternatively, CIEF can be run via application of the sample and carrier ampholytes within part of the column on the inlet side while the rest of the column is occupied by one of the electrode solutions, i.e., the catholyte or the anolyte. Such

Correspondence: Prof. Dr. Wolfgang Thormann, Institute for Infectious Diseases, CH-3008 Bern, Switzerland.
Email: wolfgang.thormann@ifik.unibe.ch

Abbreviation: **CIEF**, capillary IEF

Color online: See article online to view Figs. 1–5 in color.

a configuration permits focusing to be executed under concomitant mobilization effected by EOF [11–19], application of hydrodynamic flow, electrophoretic transport when the leading electrode solution contains a counter ion other than H_3O^+ and OH^- [18,20–25] or with combinations of these principles [18,23]. These approaches are reported to be attractive for hyphenation of CIEF with ESI-MS via use of volatile electrolytes such as formic acid and ammonium hydroxide [17,19,26] and for on-target fraction collection for offline coupling of CIEF and MALDI–MS [23]. In this context, Kilár et al. introduced a sequential injection configuration where the carrier ampholytes and samples are injected separately [16–19].

For many years, computer simulations have been conducted to understand the fundamentals and phenomena of electrophoretic processes, including IEF [27,28]. Dynamic models of various degrees of complexity have been developed, including the one-dimensional simulators GENTRANS, SIMUL5, and SPRESSO that provide identical results when used with the same input parameters [29]. Among those, GENTRANS was extensively used to describe separation dynamics of sample and ampholyte compounds in IEF, the formation and stability of the pH gradient, the electrophoretic mobilization during and after the focusing process and mobilization based on EOF [8,30–35]. In previous studies from our laboratories, simulations with GENTRANS revealed insights into sampling strategies with a sequential injection of sample and carrier ampholytes [36], the behavior of sample components with p*I* values outside the pH gradient established by carrier ampholytes [37], and conditions that lead to the formation or prevention of a pure water zone at pH 7 [38].

CIEF of components following sequential injection of carrier ampholytes and the sample was reported to offer unique advantages for analysis with UV detection and hyphenation with MS [16–19]. One paper focused on the effect of the electrolyte pH on CIEF with narrow range carrier ampholytes [18]. In that work, the sample was applied between two zones of carrier ampholytes and this triple zone pattern was bracketed by pH-adjusted electrolytes that are compatible with MS detection. Anolytes with pHs between 2.5 and 7.5 were obtained by titrating formic acid with ammonium hydroxide and catholytes with pH values between 11.0 and 7.0 were prepared by titrating ammonium hydroxide with formic acid. This kind of pH adjustment is comparable to focusing systems of the literature that feature concomitant focusing and electrophoretic mobilization [20–25]. The purpose of the work described in the present paper was to simulate selected systems with carrier ampholytes covering 2 pH units that are comparable to those of the Páger et al. study [18]. The simulations provide insight into the temporal behavior of electrolytes, carrier ampholytes, analytes, pH, and conductivity. For the first time, systems with catholytes of decreased pH, anolytes of increased pH, and both electrode solutions with adjusted pH values are simulated and compared to those with formic acid and ammonium hydroxide as anolyte and catholyte, respectively. All simulations were performed without EOF and complement previous simulations in which cathodic mobilization examples with various anions were studied only [33,34].

2 Materials and methods

2.1 Computer simulation program

For the simulations presented in this work, the previously described and employed one-dimensional electrophoresis model GENTRANS was applied [8,29–38]. This isothermal model is capable of treating weak and strong monovalent acids, bases and strong electrolytes, biprotic ampholytes, peptides, or other multivalent components, and proteins in individual modules [29]. The model is based upon the principles of electroneutrality, conservation of mass and charge, and computation of component fluxes via consideration of electromigration, molecular diffusion, and dispersion free plug flow (electroosmosis). Initial conditions that must be specified include the length of the separation space and its segmentation, the initial distribution of all components, the pKa and mobility values of each compound, the input data for electroosmosis, the current density, the species permeabilities (boundary conditions) at the ends of the separation space and the amount of electrophoresis time. The program outputs concentration, conductivity, ionic strength, and pH distributions at specified time points, as well as current density and the net flow as functions of time.

2.2 Input conditions and execution of simulations

The simulation conditions employed in this study were similar to those reported in [38] and the physico-chemical input parameters are listed in Table 1. A 10 cm focusing space divided into 10 000 segments of equal length ($\Delta x = 10$ μm) was applied. A total of 101 hypothetical biprotic carrier ampholytes ($\Delta pI = 0.02$) were used to form narrow, two-pH-unit gradients (6.00–8.00 or 7.00–9.00) between the anolyte and catholyte. For each ampholyte, ΔpKa was 2.5, the ionic mobility was 2.5×10^{-8} m^2/Vs, and the initial concentration was 200 μM. Seven sample components (p*I* 5.3, 6.4, 6.6, 7.2, 7.9, 8.6, 10.4; see Table 1 for input parameters) occupying initially 2% of column length (between 49 and 51% of the column length) were sandwiched between two equal mixtures of ampholytes (from 40% to 49% and 51% to 60% of column length). The sample zone did not contain any carrier ampholytes but 2.711 mM chloride to imitate the presence of the sample components as hydrochlorides. In the case of the 7.00 to 9.00 gradient, the carrier ampholytes contained additional 20 edge components ($\Delta pI = 0.02$, $\Delta pKa = 2.5$, 2.5×10^{-8} m^2/Vs) on both sides. The applied concentrations decreased 20% from component to component, i.e., from 160 to 2.31 μM for the components with increasing p*I*s between 9.02 and 9.40 and for the carriers with decreasing p*I*s between 6.98 and 6.60. The edge components reflect a more realistic situation of the preparations used to establish pH gradients

Table 1. Physico-chemical input parameters of sample and buffer components used in simulations[a)]

Compound	pKa_1	pKa_2	Mobility ($\times 10^{-8}$ m^2/Vs)	Initial concentration		
				Anolyte (mM)	Sample[b)] (μM)	Catholyte (mM)
pI 5.3 dye	3.70	6.90	2.00	–	463	–
pI 6.4 dye	4.68	8.12	2.00	–	398	–
pI 6.6 dye	5.10	8.10	2.00	–	520	–
pI 7.2 dye	5.70	8.70	2.00	–	368	–
pI 7.9 dye	6.81	8.99	2.00	–	329	–
pI 8.6 dye	7.70	9.50	2.00	–	281	–
pI 10.4 dye	9.50	11.30	2.00	–	352	–
Cl^-	–	–	7.91	–	2711	–
HCOOH	3.75	–	5.66	50	–	0, 2.11, 7.98, 21.92, 69.12
NH_4^+	9.25	–	7.62	0, 47.33	–	100

[a)] p*Ka* and mobility values were taken from the SIMUL5 database (http://web.natur.cuni.cz/gas/) and [38,41].
[b)] For all seven dyes, the concentrations correspond to 143 μg/mL. Dyes are injected as hydrochlorides.

and the edge components with p*I*s lower than 7 prevent the formation of a pure water zone as was discussed in our previous study [38].

Without pH adjustment, 100 mM ammonium hydroxide (pH 11.12) was used as catholyte (between 60 and 100% of column length) and 50 mM formic acid (pH: 2.54) as anolyte (between 0 and 40% of column length). For pH adjustment of the electrolytes, the desired pH values of the catholyte (pH 10.80; 10.30; 9.80; 8.90) were reached by addition of formic acid (2.11; 7.98; 21.92; 69.12 mM, respectively) to 100 mM ammonium hydroxide whereas the anolyte pH was enhanced to pH 5.00 via addition of 47.33 mM ammonium hydroxide to 50 mM formic acid. All simulations were run for 25 min of electrophoresis time at a constant current density of 200 A/m^2 and without EOF. Initial boundary widths were 0.001%, the boundary conditions were constant at both column ends, and data smoothing as described by Mosher et al. [29] was used. The program was executed on PCs featuring Intel Pentium G 870, G 2130, and Core I7 processors running at frequencies between 3.1 GHz and 3.2 GHz. Data were imported into the SigmaPlot Scientific Graphing Software Windows Version 11.0 (SPSS, Chicago, IL, USA) for making plots.

3 Results and discussion

3.1 Effects of pH adjustment of catholyte, anolyte, and both electrolyte solutions

In the work with narrow pH range ampholytes, Páger et al. [18] used anolytes with pHs between 2.5 and 7.5 and catholytes with pH values between 11.0 and 7.0 that were prepared with formic acid and ammonium hydroxide. For p*I* 6–8 carrier ampholytes, the impact of the presence of formic acid in the catholyte and ammonium hydroxide in the anolyte was studied by computer simulation. Simulation data of four situations are presented in Figure 1. They comprise one without a pH change of the electrolytes, one with the reduction of the catholyte pH, one with a higher pH change of the anolyte, and one with both electrolytes changed. Computer predicted concentration profiles of all components after 20 min of power application at a constant current density of 200 A/m^2 are depicted in the bottom panel of Figure 1, whereas corresponding conductivity and pH distributions are shown in the center and top panels, respectively, of Figure 1. In this figure, a hashtag (#) marks the region of the initial sample zone that was placed between the two zones of carrier ampholytes. In this region, electrophoretic regulation produces differences in concentration distributions, conductivity, and pH (see [36–38] for details).

In the first situation where the pH values of the catholyte and anolyte are not changed (Figure 1, graph A in bottom panel), the carrier ampholytes are depicted to form consecutive, slightly overlapping focused zones of about 9.2 mM peak concentration. The pH increases from 6.06 to 7.94 within the focusing space of 4–6 cm of the column length (Figure 1, graph A in top panel). The separation dynamics of the analytes are depicted in Figure 2A. Four amphoteric sample components become focused in the established pH gradient and produced well separated Gaussian-like foci. The p*I* 5.3, 8.6, and 10.4 analytes are predicted to establish migrating ITP zones outside the pH gradient [37]. On the cathodic side, the pI 8.6 and 10.4 analytes migrate toward the cathode behind NH_4^+, the leading cation. After 20 min of power application, they are followed by the three most basic carrier ampholytes (Figure 1, graph A in bottom panel). On the other side, the p*I* 5.3 analyte and the three most acidic carrier ampholytes form anionic ITP zones behind formate, the leading anion, and migrate toward the anode. These ongoing ITP processes result in a slow gradual decay of the pH gradient at its edges as was described previously in detail [31,32,35,37].

When the catholyte pH is reduced via addition of formic acid, formate migrates under the influence of the electric field from the catholyte through the entire focusing space. All ampholytes and samples thereby acquire a positive charge

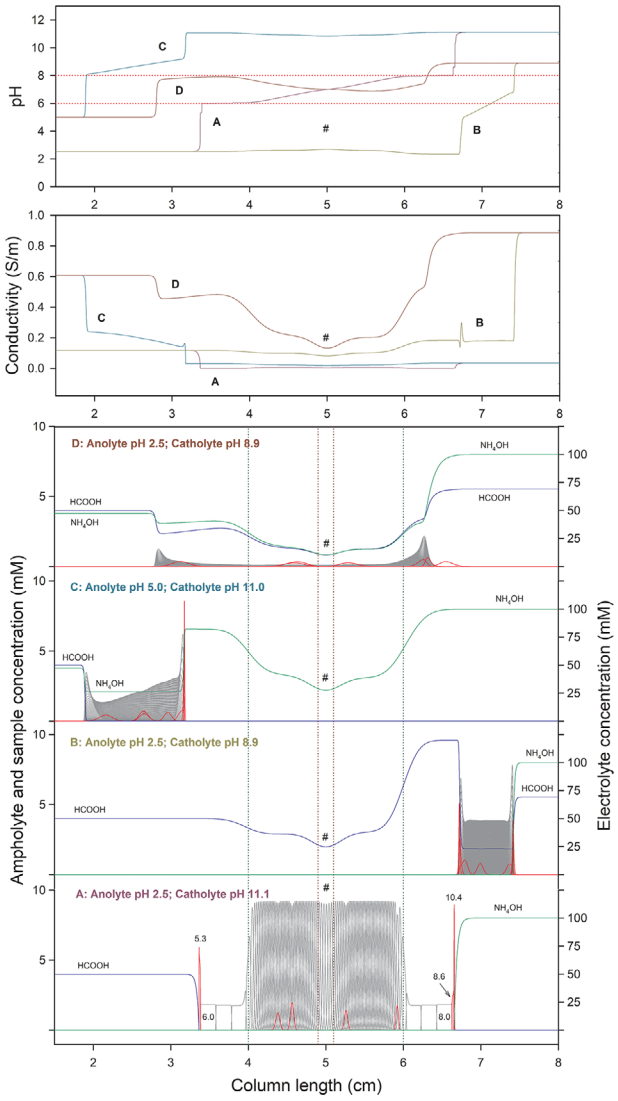

Figure 1. Computer simulated distributions of all components (bottom panel), conductivity (central panel), and pH (top panel) for the p*I* 6–8 carrier ampholytes and the seven amphoteric sample components (with p*I* values 5.3, 6.4, 6.6, 7.2, 7.9, 8.6, and 10.4) after 20 min of power application under a constant current density of 200 A/m^2. Electrolytes comprised (A) 100 mM ammonium hydroxide (pH 11.12) as catholyte and 50 mM formic acid (pH 2.54) as anolyte, (B) 69.12 mM formic acid in 100 mM ammonium hydroxide (pH 8.90) as catholyte and 50 mM formic acid (pH 2.54) as anolyte, (C) 100 mM ammonium hydroxide (pH 11.12) as catholyte and 47.33 mM ammonium hydroxide in 50 mM formic acid (pH 5.00) as anolyte, and (D) 69.12 mM formic acid in 100 mM ammonium hydroxide (pH 8.90) as catholyte and 47.33 mM ammonium hydroxide in 50 mM formic acid (pH 5.00) as anolyte. In the bottom panel, carrier ampholytes are presented as dark grey lines (*y*-axis scale to the left), sample components as red lines (*y*-axis scale to the left), formic acid as blue line (*y*-axis scale to the right), and ammonium hydroxide as green line (*y*-axis scale to the right). The dotted vertical lines mark the location of the initial boundaries between the carrier ampholytes with the sample and with the electrolytes. The dotted horizontal lines in the top panel mark pH 6.00 and 8.00. A hashtag (#) marks the region of the initial sample zone that was placed between zones of carrier ampholyte. The numbers in graph (A) represent p*I* values and demarcate the zones of the most acidic (p*I* 6.0) and most basic (p*I* 8.0) carrier ampholytes, as well as the sample components that migrate isotachophoretically outside the pH gradient. The cathode is to the right.

and hence move toward the cathode. As discussed previously, such a process forms an ITP zone structure [33]. Data obtained with a catholyte pH of 8.90 (addition of 69.12 mM formic acid to 100 mM ammonium hydroxide) and otherwise identical conditions as without pH adjustment are presented in graph B of the bottom panel of Figure 1. After 20 min of current flow, the ITP zone structure is predicted to be completely within the column segment originally filled with the catholyte with the rear and front boundaries located at 6.66 cm and 7.54 cm, respectively. The structure is bracketed by the catholyte (leading electrolyte) and a formic acid zone that becomes adjusted to 119.9 mM and acts as terminating zone with H_3O^+ as terminating ion. The role of H_3O^+ as terminating ion was described in detail by the Boček group [39,40] and is not further discussed here. Except for the front and rear parts of the ITP structure, the carrier ampholytes migrate as broadly overlapping zones of Gaussian-like shape and peak heights of around 3.8 mM. The carrier ampholytes that migrate at and close to the interfaces to the leading and terminating electrolytes form somewhat tighter peaks and thus exhibit a higher concentration. Under the current conditions, the mobility difference is insufficient to form consecutive zones of carrier ampholytes as was discussed in the example of Ref. [33]. Within the ITP structure, the formic acid concentration is around 22.9 mM (Figure 1, graph B of bottom panel), the conductivity is constant (0.181 S/m, Figure 1, graph B in center panel), and the pH gradually increases from pH 4.8 to 6.8 (Figure 1, graph B in top panel). The p*I* 6.6, 7.2, and 7.9 analytes migrate as rather broad peaks within the gradient, their peak maximum being at pH values of 5.07, 5.64, and 6.74, respectively, values that are significantly (>1 pH unit) lower compared to their p*I* values. Hence, they have a positive net charge. The analytes that migrate at the edges of the ITP structure form sharp peaks. The pI 8.6 and 10.4 analytes are at the cathodic edge, whereas the p*I* 5.3 and 6.4 analytes are at the anodic edge of the ITP stack.

The dynamics of the separating and migrating analytes are presented in Figure 2B. The initial separation is similar to that in the original setup shown in Figure 2A. At 5 min, the p*I* 6.4 and 6.6 analytes are predicted to be completely separated. At 10 min, the p*I* 6.4 analyte migrates together with the p*I* 5.3 analyte at the anodic edge of the carrier ampholyte zone. The ITP carrier ampholyte stack gradually becomes shorter that is due to the Kohlrausch adjustment occurring at the location of the initial boundary between the catholyte and the carrier ampholytes at 6 cm of column length. The migration velocity in the $x > 6$ cm is lower compared to that at $4 < x < 6$ cm. After 10 min of power application, the entire stack is almost completely within the region originally occupied by the catholyte. From then on, the length of the zone structure becomes invariant and the shape of the migrating analyte peaks remain constant.

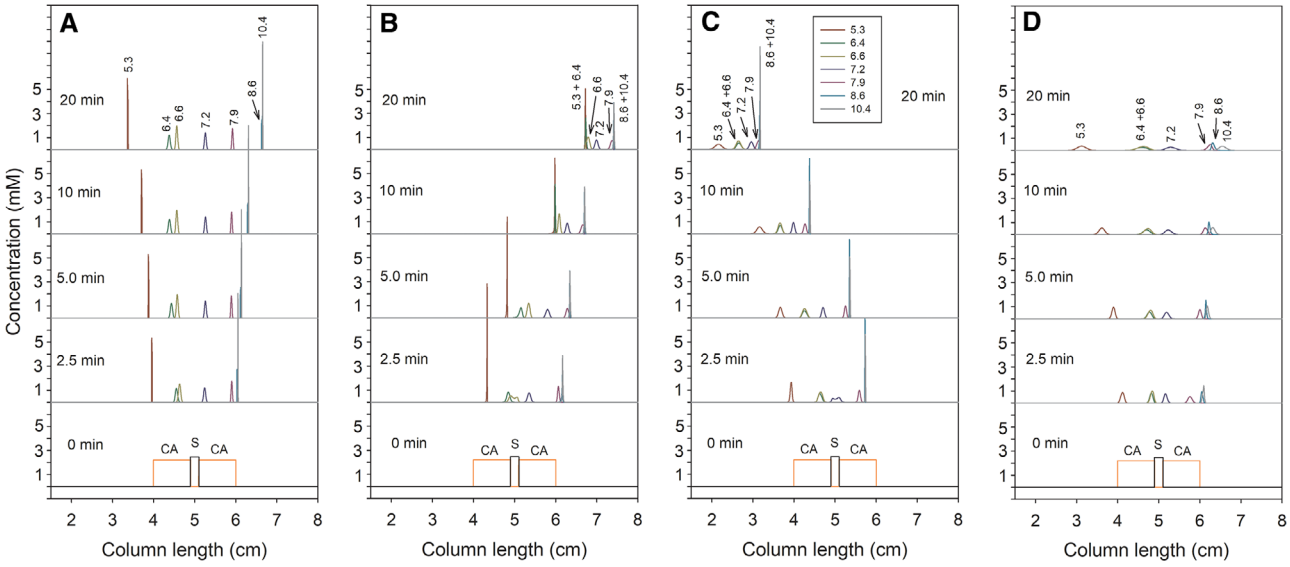

Figure 2. Computer predicted separation dynamics of the seven sample components for the four situations of Figure 1 after 0, 2.5, 5.0, 10, and 20 min of power application. The peaks in the top graphs of each panel are labelled with the pI values of the sample components. In the graphs at the bottom of each panel data are presented as the sum of the carrier component concentrations (orange line) and the sum of the analyte concentrations (black line). S and CA refer to sample and carrier ampholytes, respectively. The cathode is to the right.

When ammonium hydroxide is added to the anolyte and the catholyte remains unchanged, ammonium ions are migrating electrophoretically toward the cathode through the entire column. The ampholytes become negatively charged and an anionically migrating ITP zone structure that includes all carrier ampholytes and amphoteric analytes is formed. This is depicted in Figure 1 (graph C in bottom panel) for a situation with a pH 5.00 anolyte composed of 50 mM formic acid and 47.33 mM ammonium hydroxide. The anolyte functions as leading electrolyte with formate as the leading ion whereas the electrophoretically formed 82.10 mM ammonium hydroxide solution at the rear end of the stack acts as terminating electrolyte with OH^- being the terminating ion. The pH of the migrating gradient ranges from 7.9 to 9.2 (Figure 1, graph C in top panel) and the conductivity decreases from 0.24 to 0.14 S/m (Figure 1, graph C in center panel). All analytes migrate at a pH that is significantly higher compared to their p*I* value (pH 8.31, 8.77, 8.76, 9.04, 9.36, 9.74, and 10.77, for the analytes with p*I*s of 5.3, 6.4, 6.6, 7.2, 7.9, 8.6, and 10.4, respectively). Their dynamics is presented in Figure 2C. Simulation data reveal that the pI 5.3, 6.4, 6.6, 7.2, and 7.9 analytes migrate within the ITP stack formed by the carrier ampholytes, that the p*I* 6.4 and 6.6 analytes do not separate, and that the p*I* 8.6 and 10.6 analytes form tight ITP zones at the rear edge of the ITP stack. There is a significant overlap of the migrating carrier ampholytes. Their distribution is somewhat skewed on the anodic side that is a result of the high concentration of ammonium in relation to formate present in the anolyte. This is analogous to the situation with formate in the catholyte (Figure 1, graph B in bottom panel) for cases with 100 mM ammonium hydroxide and large amounts (>70 mM) of formic acid (data not shown).

When both electrolytes are titrated, concomitant anionic and cationic movements of carrier and sample components are predicted. This is illustrated with the data presented as graph D in the bottom panel of Figure 1. For that example, the catholyte was composed of 100 mM ammonium hydroxide and 69.12 mM formic acid (pH 8.90) whereas the anolyte comprised 50 mM formic acid and 47.33 mM ammonium hydroxide (pH 5.00). Formate is migrating from the catholyte through the entire system whereas ammonium is migrating in the opposite direction from the anolyte through the system. A non-uniform background electrolyte is thereby established (Figure 1, graph D in bottom panel). The formic acid concentration within the region occupied by the carrier ampholytes is predicted to be between 10.24 mM and 69.12 mM, while the amount of the basic component varies between 10.11 mM and 47.33. A shallow pH gradient is predicted for the region that was originally occupied by the carrier ampholytes and the sample (4–6 cm of column length, graph D in top panel of Figure 1). It is important to note that this gradient is reversed compared to those of the other three gradients, including that of the IEF system in absence of titrated electrolytes. In this complex system, carrier ampholytes and amphoteric analytes separate as cations or anions, depending on their p*I* and local pH, and do not get focused. Carrier ampholytes become distributed between anolyte and catholyte, a region that becomes longer as function of time. Carrier ampholytes that move as anions become (i) somewhat accumulated behind the buffer discontinuity that migrates toward the anode (with a concentration of up to 1.2 mM) and (ii) depleted in the region behind the buffer discontinuity that migrates toward the cathode (Figure 1, graph D in bottom panel). The opposite is true for carrier ampholytes that move toward the cathode where the accumulation behind the buffer discontinuity is

up to 2 mM. Their concentration in the central part is around 0.1 mM. The bidirectional migration of the analytes is documented with the data presented in Figure 2D. Analytes with pI < 7 migrate as anions and those with pI > 7 as cations. The pI 5.3 analyte strongly migrates toward the anode whereas the pI 6.3 and 6.4 do not separate and migrate slowly. On the cathodic side, the pI 7.2 analyte migrates slowly toward the cathode whereas the three other compounds migrate fast. Except for the last three, all analytes are predicted to migrate as broad peaks. The pI 10.4 analyte migrates within the catholyte, i.e., outside the carrier ampholytes. No ITP zone structure is formed in such a system.

3.2 Description of transition from IEF to ITP and beyond

In order to describe the transition between IEF and ITP when an electrolyte is titrated with the other electrolyte, pH 7–9 gradients established by 101 amphoteric components and additional edge ampholytes whose concentrations decrease by 20% from component to component were simulated using 100 mM ammonium hydroxide (pH 11.12) or its pH adjusted electrolytes (pH 10.8, 10.3, 9.8, and 8.9) as catholyte. Formic acid (50 mM) served as anolyte and the seven amphoteric sample components as analytes. This pH 7–9 gradient system without electrolyte modification was previously studied [38]. The graphs depicted in Figure 3 represent the computer-predicted concentration profiles of all components after 20 min of power application. Corresponding pH and conductivity data for the simulations of Figure 3 are shown in Figure 4 whereas the dynamics of the analytes for 0, 2.5, 5.0, 10, and 20 min of current flow are depicted in Figure 5.

Similar to the configuration with the pH 6–8 gradient and one-component electrolytes, simulation data show that edge components (most basic and acidic ampholytes) at the border of the established pH gradient are part of the destabilizing ITP zone structures on both sides of the pH gradient (Figure 3A). After 20 min of current flow, the pI 10.4 analyte, the 20 extra edge components and the five most basic carriers of the pI 7–9 components are part of the ITP structure on the cathodic side. On the anodic side, the ITP stack comprises the pI 5.3, 6.4, and 6.6 analytes and most of the extra edge components but none of the pI 7–9 components. The carrier ampholytes are depicted to form consecutive, slightly overlapping focused zones of about 9.2 mM peak concentration. The pH increases from 6.94 to 8.88 within the focusing space of 4 to 6 cm (Figure 4, graph A in upper panel). The pI 7.2, 7.9, and 8.6 analytes are predicted to be focused in the established pH gradient (Figure 5A).

When the catholyte is titrated to pH 10.8 with 2.11 mM formic acid (Figure 3B), formate is migrating through the entire region with the carrier and sample components that thereby become mobilized toward the cathode via formation of an ITP zone structure. The carrier ampholytes separated and established a train of consecutive ITP peaks between the catholyte (leading electrolyte) and 24.7 mM formic acid

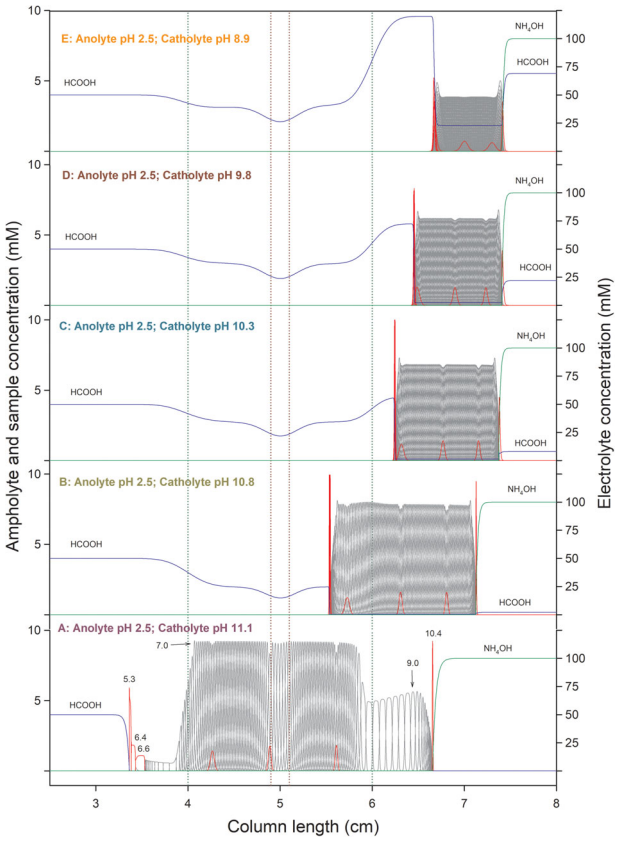

Figure 3. Computer simulated concentration distributions of all components for systems with the p*I* 7.0–9.0 carrier ampholytes, 20 additional edge carrier ampholytes on both sides, and the seven amphoteric sample components after 20 min of power application under a constant current density of 200 A/m^2. The catholytes comprised (A) 100 mM ammonium hydroxide (pH 11.12), (B) 2.11 mM formic acid in 100 mM ammonium hydroxide (pH 10.80), (C) 7.98 mM formic acid in 100 mM ammonium hydroxide (pH 10.30), (D) 21.92 mM formic acid in 100 mM ammonium hydroxide (pH 9.80), and (E) 69.12 mM formic acid in 100 mM ammonium hydroxide (pH 8.90). The anolyte was 50 mM formic acid (pH 2.54) in all cases. The numbers in graph A represent pI values and demarcate the zones of the pI 7.0 and pI 9.0 carrier ampholytes, as well as the sample components that migrate isotachophoretically outside the pH gradient. Other conditions as for Figure 1.

(terminating electrolyte). The overall distribution of the ampholytes is somewhat shorter compared to the case in IEF whose data are in Figure 3A. After 20 min of current flow, the front boundary is at 7.1 cm whereas the rear boundary at 5.5 cm. The ITP stack is composed of two sections, one between 6 cm and the front boundary (area that was first occupied by the catholyte) and one between the rear boundary and 6 cm (area that was originally occupied with carrier ampholytes). Due to the Kohlrausch adjustment occurring at x = 6 cm the properties of the two sections of the migrating ITP peaks are slightly different. The formic acid concentration in the first and second section are 0.44 and 0.36 mM, respectively. The peak concentration of the migrating carrier ampholytes is about 7.8 and 8.0 mM, respectively. The reason for the lower concentration compared to the 9.3 mM in

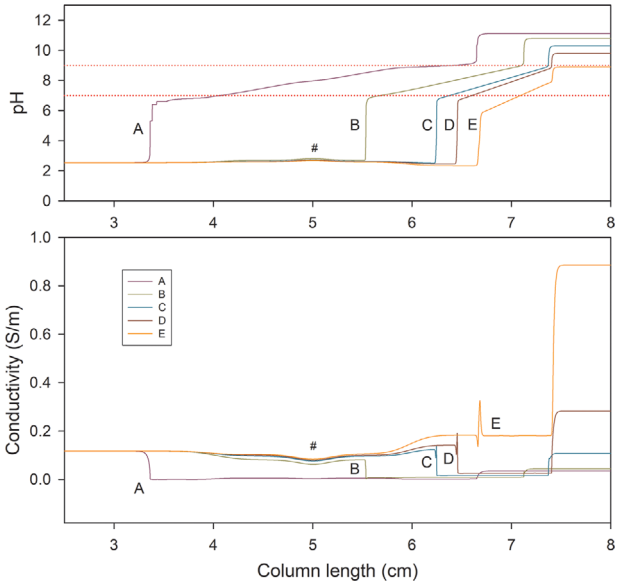

Figure 4. Simulated conductivity profiles (lower panel) and pH data (upper panel) for the five systems of Figure 3. The dotted red horizontal lines in the upper panel mark pH 7.00 and 9.00. A hashtag (#) marks the region of the initial sample zone that was placed between zones of carrier ampholyte. The cathode is to the right. Other conditions are the same as for Figure 3.

the case of IEF is that the ITP boundaries are broader compared to the concentration gradients in IEF. Thus, there is more ampholyte overlap in ITP compared to IEF. The conductivities within the two sections are low and almost constant (about 7.27 × 10^{-3} and 8.88 × 10^{-3} S/m, respectively, graph B in lower panel of Figure 4). The span of the pH gradient is comparable to that of IEF (Figure 4, graph B in upper panel). The p*I* 5.3, 6.4, and 6.6 analytes are tightly focused at the anodic end of the ITP zone structure whereas the p*I* 10.4 analyte is at the cathodic end. The p*I* 7.2, 7.9, and 8.6 analytes are well separated and migrate as ITP peaks within the carrier ampholytes. Their shapes are comparable to those encountered in IEF (compare data of Figure 5B with those of 5A). In the case of ITP, however, the analytes, are not in their isoelectric state but are partially positively charged. After 20 min of current flow, the rear boundary is at 5.5 cm (Figures 3B and 5B). At this time, the uniform ITP structure with the characteristics of the first section is not yet complete and the pI 7.2 analyte became tighter (Figure 5B).

With an increase of the formic acid concentration in the catholyte, a higher transport rate of all carriers and samples together with a shrinkage of the migrating ITP structure is predicted. Simulation examples with pH 10.30, 9.80, and 8.90 catholytes comprising 7.98 mM, 21.92 mM, and 69.12 mM formic acid, respectively, in 100 mM ammonium hydroxide are presented in Figure 3C–E, respectively. Corresponding pH and conductivity data are depicted in Figure 4 whereas the dynamics of the analytes are shown as panels C–E, respectively, of Figure 5. For the three cases, carrier ampholyte peaks decrease (6.83 mM, 6.18 mM and 3.87 mM, respectively) and the overlap of neighboring carriers increases. Furthermore, the formic acid within the ITP structure increases (1.32 mM, 2.45 mM and 22.9 mM, respectively) and its concentration in the terminating electrolyte becomes 55.6 mM, 72.4 mM and 119.9 mM, respectively. The increase of the formic acid concentration in the catholyte results in an increase in the conductivity (Figure 4, graphs C–E in lower panel), a decrease of the pH gradient span (Figure 4, graphs C–E in upper panel) and a lower resolution of the analytes (Figure 5, panels C–E).

These simulation data illustrate that (i) a low millimolar concentration of formic acid in the 100 mM ammonium hydroxide catholyte is sufficient to mobilize the entire gradient formed with carrier ampholytes covering 2 pH units toward the cathode, and (ii) resolution of amphoteric analytes becomes lower as the amount of formic acid is increased. Although the data shown here describe electrophoretic mobilization toward the cathode, all conclusions reached are also valid for anodic mobilization, i.e., using an anolyte with two components (e.g., ammonium hydroxide in formic acid) together with a base as catholyte. Furthermore, it is important to mention that the uptake of carbon dioxide by the catholyte has a comparable effect as the addition of a small amount of ammonium hydroxide or another base to the catholyte. This is discussed in detail elsewhere [35,38]. A more concise way to analyze the formed ITP systems would be a description with effective mobilities that would reveal analytes that are stacked at the leading or terminating boundary, migrate within the ampholyte zone, or not become stacked at all. This approach is based on the fundamental work of the Boček group [39,40], is not considered here, and should be the subject of further work.

3.3 Comparison of simulation and experimental data

Simulation data obtained without pH adjustment were found to compare well with those of the experimental study of Páger et al. [18]. In the IEF situations with one-component electrolytes, amphoteric analytes separate due to differences in p*I* values. The p*K*a and thus the p*I* values of the dyes used for the simulations were those determined experimentally and reported in the literature [41]. Thus, separation patterns predicted by simulation are in qualitative agreement with those monitored experimentally. In this context, it is important to realize that the experiments of Páger et al. [18] were performed in uncoated fused-silica capillaries under the action of EOF that enables the detection of the analytes with a single detector placed toward the capillary end. The experimental data format is time-based that is different compared to the distance-based simulations presented in this paper. In the electropherograms, the most alkaline sample component is thus detected first. The EOF in systems with discontinuous buffers and electrolytes, such as those encountered in IEF and ITP, is not constant and difficult or even impossible to simulate [34,42]. Thus, the measured resolution of analytes cannot be compared with that predicted in our simulations.

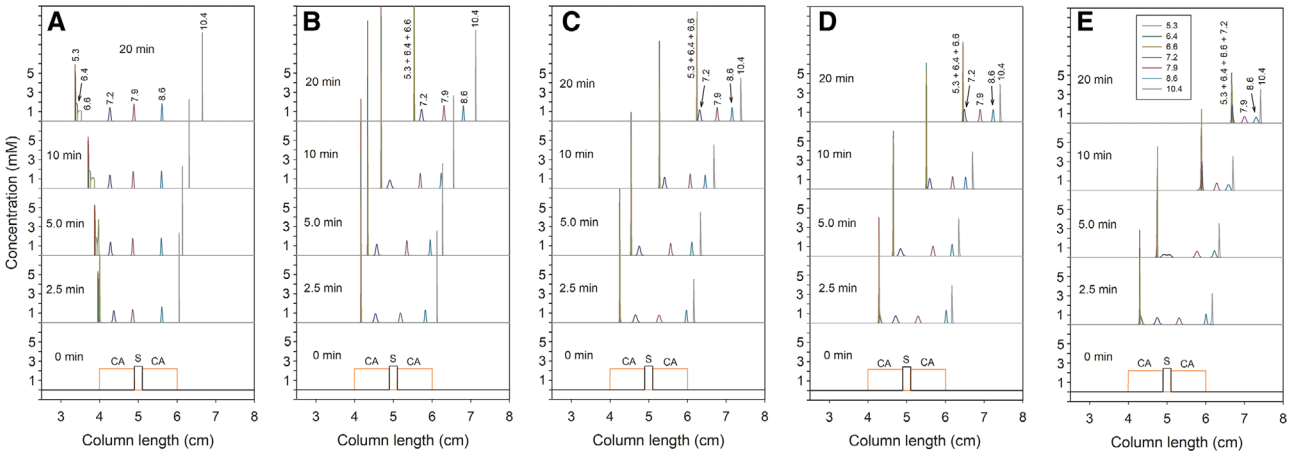

Figure 5. Computer predicted separation dynamics of the seven sample components for the five systems of Figure 3 after 0, 2.5, 5.0, 10, and 20 min of power application. The cathode is to the right. Other conditions as for Figure 2.

The order of analytes within the pattern, however, is not affected by EOF.

Simulation predicts that addition of formic acid to the catholyte comprising 100 mM ammonium hydroxide induces the formation of an ITP zone structure that contains all ampholytes, i.e., carrier components and anolytes. Data for p*I* 7–9 carrier ampholytes is presented in Figure 3. Situations without and with 21.92 mM formic acid (Figure 3A and D, respectively) correspond to the experimental data depicted in Figure 1A and B, respectively, of Páger et al. [18]. In both cases the amphoteric analytes are detected and predicted to be located within or at the edges of the carrier ampholyte zone. The order of appearance of the analytes is the same. In the case of IEF, the carrier ampholyte concentration is higher compared to that of the ITP zone, a fact that is also predicted by simulation. Furthermore, with a lower load of carrier ampholytes, a shorter overall pattern is experimentally detected (compare data of Figure 1C with those of Figure 1B in Páger et al. [18]). This behavior corresponds to ITP where the zone length is proportional to the amount sampled. This is not the case in IEF. Thus, it can be concluded that the patterns in Figure 1B and C of Páger et al. [18] represent ITP zone structures which is in agreement with simulations.

In both, the simulations and the experiments, a decrease in pH of the catholyte or increase of the anolyte pH resulted in positively or negatively charged ampholytes and the formation of an isotachophoretic ampholyte zone structure migrating toward the cathode and anode, respectively. In ITP, separation of analytes occurs according to differences in electrophoretic mobilities. As the mobilities of the applied amphoteric analytes were not available from the literature and were not determined in our laboratories, simulations were performed with an estimated mobility of 2.0×10^{-8} m^2/Vs (Table 1). This essentially resulted in an ITP migration order according to their p*I* values (Figures 2 and 5) and does not necessarily reflect reality as the actual mobilities of analytes with similar p*I* values can be such that they migrate in reversed order of the p*I*s or become inseparable (cf. p*I* 6.4 and 6.6 analytes [18]). The same can be true for situations in which the catholyte and the anolyte are both modified. The simulation data presented in Figures 1D and 2D are in qualitative agreement with those monitored experimentally (compare with data of Figure 6B in Páger et al. [18]). The p*I* 10.4 analyte migrates within the catholyte. In the simulation, the p*I* 6.4 and 6.6 analytes are predicted to be inseparable. In the experiment, a broad zone was detected.

4 Concluding remarks

The work described in this paper represents another application in which dynamic simulation is used to provide valuable insight into the dynamics of all components, pH, and conductivity of specific electrophoretic systems. The focus was on carrier ampholytes covering 2 pH units and pH-adjusted volatile electrolytes that are comparable to those of the Páger et al. study [18] in which the electrolytes were composed of formic acid and ammonium hydroxide. For the first time, the electrophoretic behavior of systems with catholytes of decreased pH, anolytes of increased pH, and both electrode solutions with adjusted pH values were studied by computer simulation, and the results were compared to those with formic acid and ammonium hydroxide as anolyte and catholyte, respectively. Without modification, simulation is demonstrated to provide the expected IEF system. Analytes with p*I* values within the formed pH gradient are focused and become immobile. Addition of formic acid to the catholyte (decrease of its pH) results in an ITP system that is bracketed by the catholyte and formic acid on its cathodic and anodic sides, respectively, and migrates toward the cathode. With addition of ammonium hydroxide to the anolyte (increase of its pH) an ITP system migrating toward the anode is produced. The ITP stack is bracketed by the anolyte and a formed ammonium hydroxide terminator. In the two ITP cases, all analytes migrate isotachophoretically as cations or anions, respectively. When both electrolytes are titrated, concomitant

anionic and cationic movements of carrier and sample components are predicted. A non-uniform background electrolyte composed of formic acid and ammonium hydroxide is established in which analytes migrate according to local pH and conductivity without forming IEF or ITP zone structures. For selected examples, the simulation data are shown to be in qualitative agreement with those monitored experimentally by Páger at al. [18].

The data presented reveal that millimolar amounts of a charged additive to a 100 mM electrolyte are sufficient to convert an IEF pattern into an ITP system and this without significant alteration of the pH gradient. The impact of the uptake of carbon dioxide by the catholyte has a comparable effect [35,38]. With increased amounts of the added counter ion, however, the range of the migrating pH gradient changes, the overall length of the ITP structure decreases which is associated with a loss of resolution, and the migration rate of the structure increases. The studied examples indicate that systems of this type should be classified as ITP and not IEF. The same is true for systems with another base added to the catholyte (or another acid to the anolyte) and has to be taken into account for all electrophoretic systems that feature concomitant focusing and electrophoretic mobilization. Various examples of this type of ITP separations are found in the literature [20–25,33,34].

This work was supported by TÁMOP-4.2.2.D-15/1/KONV-2015-0015, NKFIH K-125275, and the Swiss NSF.

The authors have declared no conflict of interest.

Data availability statement

The data that support the findings of this study are available from the corresponding author upon reasonable request.

5 References

[1] Righetti, P.G., *Isoelectric Focusing: Theory, Methodology and Applications*, Elsevier, Amsterdam, 1983.

[2] Hjertén, S., Zhu, M., *J. Chromatogr.* 1985, *346*, 265–270.

[3] Hjertén, S., Liao, J., Yao, K., *J. Chromatogr.* 1987, *387*, 127–138.

[4] Zhu, M., Rodriguez, R., Wehr, T., *J. Chromatogr.* 1991, *559*, 479–488.

[5] Rodriguez-Diaz, R., Wehr, T., Zhu, M., *Electrophoresis* 1997, *18*, 2134–2144.

[6] Manabe, T., Miyamoto, H., Iwasaki, A., *Electrophoresis* 1997, *18*, 92–97.

[7] Mack, S., Cruzado-Park, I., Chapman, J., Ratnayake, C., Vigh, G., *Electrophoresis* 2009, *30*, 4049–4058.

[8] Thormann, W., Mosher, R.A., *Electrophoresis* 2008, *29*, 1676–1686.

[9] Thormann, W., Tsai, A., Michaud, J.-P., Mosher, R.A., Bier, M., *J. Chromatogr. A* 1987, *389*, 75–86.

[10] Wu, J., Pawliszyn, J., *Electrophoresis* 1995, *16*, 670–673.

[11] Mazzeo, J.R., Krull, I.S., *Anal. Chem.* 1991, *63*, 2852–2857.

[12] Thormann, W., Caslavska, J., Molteni, S., Chmelík, J., *J. Chromatogr. A* 1992, *589*, 321–327.

[13] Molteni, S., Frischknecht, H., Thormann, W., *Electrophoresis* 1994, *15*, 22–30.

[14] Caslavska, J., Molteni, S., Chmelík, J., Šlais, K., Matulík, F., Thormann, W., *J. Chromatogr. A* 1994, *680*, 549–559.

[15] Moorhouse, K.G., Eusebio, C.A., Hunt, G., Chen, A.B., *J. Chromatogr. A* 1995, *717*, 61–69.

[16] Kilár, F., Végvári, Á., Mód, A., *J. Chromatogr. A* 1998, *813*, 349–360.

[17] Páger, C., Dörnyei, Á., Kilár, F., *Electrophoresis* 2011, *32*, 1875–1884.

[18] Páger, C., Vargová, A., Takácsi-Nagy, A., Dörnyei, Á., Kilár, F., *Electrophoresis* 2012, *33*, 3269–3275.

[19] Páger, C., Biherczova, N., Ligetvári, R., Berkics, B.V., Pongrácz, T., Sándor, V., Bufa, A., Poór, V., Vojs Stanova, A., Kilár, F., *J. Sep. Sci.* 2017, *40*, 4825–4834.

[20] Jenkins, M.A., Ratnaike, S., *Clin. Chim. Acta* 1999, *289*, 121–132.

[21] Zhang, C.-X., Xiang, F., Paša-Tolić, L., Anderson, G.A., Veenstra, T.D., Smith, R.D., *Anal. Chem.* 2000, *72*, 1462–1468.

[22] Chartogne, A., Reeuwijk, B., Hofte, B., van der Heijden, R., Tjaden, U.R., van der Greef, J., *J. Chromatogr. A* 2002, *959*, 289–298.

[23] Chartogne, A., Gaspari, M., Jespersen, S., Buscher, B., Verheij, E., van der Heijden, R., Tjaden, U., van der Greef, J., *Rapid Commun. Mass Spectrom.* 2002, *16*, 201–207.

[24] Lopez-Soto-Yarritu, P., Díez-Masa, J.C., Cifuentes, A., de Frutos, M., *J. Chromatogr. A* 2002, *968*, 221–228.

[25] Lacunza, I., Díez-Masa, J.C., de Frutos, M., *Electrophoresis* 2007, *28*, 1204–1213.

[26] Hühner, J., Lämmerhofer, M., Neusüß, C., *Electrophoresis* 2015, *36*, 2670–2686.

[27] Thormann, W., Breadmore, M. C., Caslavska, J., Mosher, R.A., *Electrophoresis* 2010, *31*, 726–754.

[28] Thormann, W., Mosher, R.A., *Electrophoresis* 2022, *43*, 10–36. https://doi.org/10.1002/elps.202100191.

[29] Mosher, R.A., Breadmore, M.C., Thormann, W., *Electrophoresis* 2011, *32*, 532–541.

[30] Mosher, R.A., Saville, D.A., Thormann, W., *The Dynamics of Electrophoresis*, VCH Publishers, Weinheim 1992.

[31] Mao, Q., Pawliszyn, J., Thormann, W., *Anal. Chem.* 2000, 5493–5502.

[32] Mosher, R.A., Thormann, W., *Electrophoresis* 2002, *23*, 1803–1814.

[33] Thormann, W., Mosher, R.A., *Electrophoresis* 2006, *27*, 968–983.

[34] Thormann, W., Caslavska, J., Mosher, R.A., *J. Chromatogr. A* 2007, *1155*, 154–163.

[35] Thormann, W., Mosher, R.A., *Electrophoresis* 2021, *42*, 814–833.

[36] Takácsi-Nagy, A., Kilár, F., Páger, C., Mosher, R.A., Thormann, W., *Electrophoresis* 2012, *33*, 970–980.

[37] Thormann, W., Kilár, F., *Electrophoresis* 2013, *34*, 716–724.

[38] Takácsi-Nagy, A., Kilár, F., Thormann, W., *Electrophoresis* 2017, *38*, 677–688.

[39] Boček, P., Gebauer, P., Deml, M., *J. Chromatogr.* 1981, *219*, 21–28.

[40] Gebauer, P., Boček, P., *J. Chromatogr.* 1983, *267*, 49–65.

[41] Šlais, K., Friedl, Z., *J. Chromatogr. A* 1994, *661*, 249–256.

[42] Thormann, W., Zhang, C.-X., Caslavska, J., Gebauer, P., Mosher, R.A., *Anal. Chem.* 1998, *70*, 549–562.

